Valence calculations of lanthanide anion binding energies: 6*p* and 6*s* attachments to $4f^m(5d+6s+6p)^3$ thresholds

Steven M. O'Malley and Donald R. Beck
Physics Department, Michigan Technological University, Houghton, Michigan 49931, USA
(Received 7 November 2008; published 23 January 2009)

Relativistic configuration-interaction calculations have been performed for anion states representing 6*p* attachments to $4f^m5d6s^2$ states in Gd and Tb as well as 6*s* attachments to $4f^m5d^26s$ thresholds in Pr and Gd. The 4*f* subshell was treated as corelike with the same occupancy in all correlation configurations, and recently developed methods for reducing the complexity of the $4f^m$ subgroup were also employed. Results predict a single weakly bound (24 meV) even state for Pr^-, 12 even states and three odd states for Gd^- (the lowest level having an electron affinity of 234 meV), and six odd states for Tb^-. The lowest $4f^85d6s^26p$ Tb^- state is bound relative to the neutral $4f^96s^2$ ground state by 88 meV, indicating that the Tb^- ground state may actually be an attachment to the first excited state of the neutral atom. Revised calculations and analyses of the much simpler Lu^-, La^-, and Ce^- anions are also presented.

DOI: 10.1103/PhysRevA.79.012511 PACS number(s): 32.10.Hq, 31.15.am, 31.15.ve, 31.15.vj

I. INTRODUCTION AND MOTIVATION

Recent developments in our relativistic configuration-interaction (RCI) methodology [1,2] have focused on limiting the size of our computational bases through universal *jls* restrictions of electron subgroups. This approach has been applied to 6*p* attachments to lanthanide $4f^n6s^2$ ground-state configurations by treating the 4*f* subshell as corelike and retaining the same occupancy (*n*) and *jls* composition of the $4f^n$ subgroup in every correlation configuration. These calculations [2] predicted a linear decrease in electron affinity (EA) with increasing *n* for Pr^- ($n=3$, 177 meV) through Tm^- ($n=13$, 22 meV), excluding Gd^-. The work presented here is an expansion of this methodology to anion states representing attachments to $4f^m(5d+6s+6p)^3$ neutral thresholds, where $m \equiv n-1$. In general, these configurations represent an increase in the complexity of the RCI calculations, since the neutral thresholds now have a valence three-electron subgroup (roughly as computationally difficult as the $4f^n6s^26p$ anion cases), and the anion $4f^m5d6s^26p$ and $4f^m5d^26s^2$ calculations now have a valence four-electron subgroup.

For a comprehensive survey of the lanthanide anions, it is useful to consider types of electron attachments and expected binding energies (BEs). We have long used the computational strategy of treating *d* attachments to neutral $d^{k-1}s^2$ ground states as *s* attachments to excited d^ks thresholds [3–5] to avoid difficulties of differing *d* occupancy between neutral and anion calculations (reducing the importance of core-valence correlation). However, the example of the Ce^- ground state, whose *LS* composition (^4H primary, ^2G secondary) [6,7] suggests a literal 6*s* attachment to $4f5d^26s$ ^5H, has led us to consider the position of these d^ks thresholds as paramount when attempting to attach *d* electrons to ground states. Analysis of *s* attachments in transition metals [8,9] yields a linear trend in BE (excluding $k=3$ to $k=5$), though it is unclear whether $k=2$ should necessarily follow this linear relation, since the relative *s* bindings of d^2s^2 for the first two series do not produce bound anion states. Their predicted relative *s* binding is ~0.65 eV in both cases, but the lowest d^2s $^4F_{3/2}$ thresholds in Sc and Y are at 1.428 eV [10] and 1.356 eV [11], respectively, so anions in both cases are only created by *p* attachments to the ds^2 ground-state configurations [12]. Since the predicted relative *s* binding in the third transition series is ~0.84 eV for La^- [8], and our own reinterpretation [7] of experimental data [13] in Ce^- gives an *s* binding of ~0.95 eV relative to $4f5d^26s$ $^5H_3$, we have considered potential 6*s* attachments to lanthanide states with open 6*s* configurations within ~1.0 eV of the neutral ground state. Similarly, since 6*p* attachments to lanthanide ground states have been found to be less than 0.5 eV [2,14–17], we have considered potential 6*p* attachments to any lanthanide state within ~0.5 eV of the neutral ground state.

In Table I we list energies for the lowest identified [10,18] levels of several configurations for all the lanthanide elements. Not all the configurations are relevant for all elements, but the energies have been included here for completeness and to illustrate that most of these manifolds are much too high ($\geqslant$1.5 eV) to be viable attachment thresholds. The choice of configurations are those with open 6*s* subshells and those that are potential thresholds for photodetachment from expected bound states that could be seen by laser photodetachment electron spectroscopy (LPES) [19] or tunable laser photodetachment threshold spectroscopy (LPTS) [20] experiments. For example, 6*p* attachments to $4f^m5d6s^2$ states could detach the 6*p* electron ($6p \rightarrow \epsilon s + \epsilon d$) back to that same configuration, or they could detach to $4f^m5d6s6p$ ($6s \rightarrow \epsilon p$) or $4f^m6s^26p$ ($5d \rightarrow \epsilon p + \epsilon f$) thresholds (it is also possible to detach to $4f^m5d^26s$ thresholds due to 3%–8% mixing of the $4f^m5d^26s6p$ configuration in these anion states, though these partial cross sections are likely much smaller).

Our earlier calculations [1,2] involving attachments to $4f^n$ configurations found that $4f^n5d6s^2$ states in Pr^- and Nd^- were unbound by ~0.2 eV, confirming that 6*s* attachments relative to the $4f^n5d6s$ thresholds (1.002 eV and 1.051 eV, respectively) have relative bindings of 0.8–0.9 eV. Similarly, in this study some preliminary calculations found that a 6*s* attachment to the Nd $4f^35d^26s$ threshold at 1.091 eV was also unbound relative to the Nd ground state by 0.2–0.3 eV. Given the consistency of these bindings (less than 1.0 eV), we have not attempted the much more complicated attach-

 ©2009 The American Physical Society

TABLE I. Survey of attachment (and photodetachment) thresholds of neutral lanthanide atoms with the energy of the lowest level of each configuration given in eV [10,18]. The notation "g.s." indicates the ground-state configuration, "n.a." indicates states that are not applicable in Lu ($n=15$), and "?" denotes configurations not identified by experiment [10,18] (Pm, which has no stable isotope, is less well known than the other lanthanides, but its unidentified levels begin at 2.121 eV).

Atom	n (m)	$4f^m6s^2$	$4f^m5d6s^2$	$4f^m5d6s$	$4f^m6s6p$	$4f^m5d^26s$	$4f^m6s^26p$	$4f^m5d6s6p$
La	1 (0)	1.884	g.s.	2.910	3.564	0.331	2.018	1.644
Ce	2 (1)	0.591	g.s.	1.502	2.267	0.294	1.929	1.676
Pr	3 (2)	g.s.	0.550	1.002	1.665	0.832	2.398	2.247
Nd	4 (3)	g.s.	0.839	1.051	1.695	1.091	?	2.513
Pm	5 (4)	g.s.	?	?	?	?	?	?
Sm	6 (5)	g.s.	2.241	1.339	1.711	2.832	?	?
Eu	7 (6)	g.s.	3.453	1.602	1.744	3.869	?	?
Gd	8 (7)	1.357	g.s.	3.007	3.181	0.791	1.666	1.740
Tb	9 (8)	g.s.	0.035	1.872	1.846	1.015	1.688	1.860
Dy	10 (9)	g.s.	0.938	2.172	1.930	2.290	2.556	2.856
Ho	11 (10)	g.s.	1.039	2.339	1.966	2.500	2.303	2.990
Er	12 (11)	g.s.	0.890	2.401	2.024	2.500	2.041	2.849
Tm	13 (12)	g.s.	1.627	2.530	2.076	?	2.786	3.634
Yb	14 (13)	g.s.	2.875	3.036	2.143	4.639	3.976	4.945
Lu	(14)	n.a.	g.s.	n.a.	n.a.	2.337	0.513	2.161

ment to the Tb $4f^85d^26s$ threshold at 1.015 eV.

Besides $6p$ attachments to the $4f^m5d6s^2$ ground states in this study we also considered the $4f^26s^2$ ($n=2$, 0.591 eV) threshold in Ce and the $4f^25d6s^2$ ($m=2$, 0.550 eV) threshold in Pr. These calculations assume negligible mixing between manifolds of differing $4f$ occupancy, so this Ce^- odd calculation does not include the $4f5d^26s^2$ Ce^- ground-state configuration or its largest correlation configurations. Nevertheless, it is interesting to find that the final calculation places this Ce^- state above the Ce ground state, but bound relative to its threshold by 190 meV in good agreement with the extrapolation of the $4f^m6s^26p$ data [2], which predicts a value of 197 meV. Preliminary calculations for this Pr^- $6p$ attachment suggest it is bound to the 0.550 eV threshold by less than 0.3 eV, as might be expected by the highest BE (300 meV [7]) of the $6p$ attachments to the Ce ground state.

The goal of this current study is then to calculate BEs for attachments to the remaining likely lanthanide thresholds. This includes $6p$ attachments to $4f^m5d6s^2$ states in Gd (ground state) and Tb (0.035 eV) as well as $6s$ attachments to $4f^m5d^26s$ states in Pr (0.832 eV) and Gd (0.791 eV). We also revisit the ends of the lanthanide row, Lu^-, La^-, and Ce^-, as a means of estimating the accuracy of our limited basis sets in these complicated calculations near the center of the row. Finally, we include here the $6p$ attachment to the Lu $6s^26p$ threshold at 0.513 eV, which has higher binding (>0.5 eV) relative to its threshold due to the double occupancy of the $6p$ subshell in the Lu^- $6s^26p^2$ $^3P_0$ state. This state was not explored in our earlier work [15], but it was previously predicted bound by 93 meV by Eliav *et al.* [21].

II. METHODOLOGY

A. One-electron wave functions

Our one-electron wave functions are generated by the multiconfigurational Dirac-Fock (MCDF) code of Desclaux [22], with both neutral and anion calculations including configurations representing all single and double replacements among the $5d$, $6s$, and $6p$ subshells. When treating $4f^m5d^26s^2$ anion states as $6s$ attachments to $4f^m5d^26s$, we usually select a higher neutral total J such that $4f^m5d6s^2$ is absent and the $4f^m5d^26s$ reference level is the lowest state of that J. Subshells not present in the above MCDF configurations are represented in RCI correlation configurations by screened hydrogenic "virtual" orbitals, denoted vl. As each virtual subshell is added to the RCI calculations, it is necessarily orthogonalized to all DF and prior virtual orbitals of the same symmetry, and its effective charge, Z^*, is determined via energy minimization.

For the $6p$ attachments, generating MCDF $6p$ radial functions for the $4f^m5d6s^2$ neutral states is needed to ensure the same level of radial basis saturation between neutral and anion calculations. For the $6s$ attachments, where $6p$ is not present in the principle configuration of either the anion or the neutral states, we find that a DF $6p$ optimized to the $6s^2\rightarrow p^2$ correlation configuration in the anion calculation then allows the first vp orbital to optimize the $5d6s\rightarrow pf$ configuration. This alleviates potential problems [5] with choosing between two very different first vp Z^*'s and leads to faster radial basis saturation than test calculations using only vp, vp', etc.

We have also recently [1,2] focused on blending of one-electron radial bases that are optimized to different anion states. This is somewhat different that the weighted average of states or use of different bases for multiple states that are used by some other practitioners of the MCDF methodology [23,24]. Here we simply "swap out" orbitals generated from two different MCDF calculations optimized to different relativistic configurations. The $6p$ attachments are the most critical example, where we find that optimizing to a state that is predominantly a $6p_{1/2}$ attachment to a neutral threshold re-

sults in quite different $\langle r \rangle$ for the two $6p$ radial functions, e.g., 6.7 a.u. versus 4.9 a.u. for $6p_{1/2}$ and $6p_{3/2}$ in Gd^- $4f^7 5d6s^2 6p$ calculations. Including $4f^m 5d6p^3$ is important in generating an MCDF solution, as multiple occupation of the $6p_{1/2}$ orbital in $4f^m 5d6p_{1/2}^2 6p_{3/2}$ helps bind this electron to the neutral core, but the $6p_{3/2}$ radial then tends to have an $\langle r \rangle$ similar to $6s$ due to $4f^m 5d6p_{1/2}6p_{3/2}^2$ $(6s^2 \rightarrow 6p_{3/2}^2)$. A separate calculation optimized to another level or a different J, where the state is predominantly a $6p_{3/2}$ attachment to $4f^m 5d6s^2$, results in flipping of the more diffuse radial between $6p_{3/2}$ and $6p_{1/2}$, and our hybrid basis set then uses the diffuse radial function from two separate MCDF calculations. While the core radials of the two calculations are similar, the swapped $6p_{3/2}$ function is nevertheless orthogonalized to $2p_{3/2}$ through $5p_{3/2}$ at the start of the RCI calculation.

The impact of the hybrid basis on the RCI energy levels of excited states is immediately apparent in even a small few-configuration test calculation. Configurations representing single electron replacements of the same symmetry in our RCI calculations are considered a gauge of the quality of our one-electron basis, and $6p \rightarrow vp$ can contribute as much as 0.4 eV in excited $6p_{3/2}$ attachment states when using radial functions optimized to a $6p_{1/2}$ level. With the hybrid basis using both diffuse $6p$ radial functions, $6p \rightarrow vp$ typically contributes $\sim$25 meV or less in all levels of interest, i.e., the bulk of the 0.4 eV is now in the MCDF energy of the upper states since $4f^m 5d6s^2 6p$ is a much better zeroth-order approximation for both types of attachments. Comparison of the $6p$ radial wave functions for the lanthanides in this study are presented in Fig. 1, where the major components of both radials from a $6p_{1/2}$ MCDF calculation are shown along with $6p_{3/2}^*$, the diffuse radial from a $6p_{3/2}$ calculation.

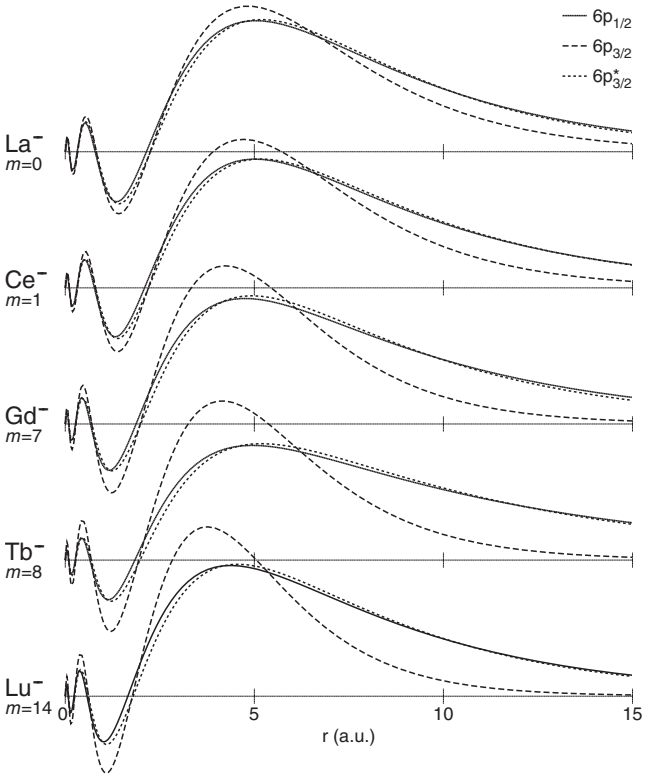

FIG. 1. One-electron radial $6p$ wave functions (major components) from $4f^m 5d6s^2 6p$ calculations. The more compact $6p_{3/2}$ functions from the basis sets that are optimized to $6p_{1/2}$ attachments are swapped out for the $6p_{3/2}^*$ functions which are optimized to $6p_{3/2}$ attachments.

B. Many-electron wave functions

Our many-electron RCI basis functions are eigenstates of J^2, J_z, and parity and are linear combinations of antisymmetrized determinants of the one-electron basis functions. For these calculations we include two sets of virtual orbitals up to $l=3$ (vf) with all first-order correlation configurations, i.e., single and double replacements with j restrictions on vl^2 or $vlvl'$ subgroups based on the DF subshells being replaced. Second-order effects including triple and quadruple replacements, as well as configurations representing relaxations of the above j restrictions, are tested on a case by case basis. Those that contribute $\sim$2 meV or more to the anion or neutral energies (due to interaction with important first-order configurations) are kept in the final calculations using the first set of virtual orbitals only; typically 15–20 such types of large second-order effects are present.

The improvements of the one-electron radial bases discussed in Sec. II A result in rapid saturation of the radial space with total increased binding of anion states due to the second set of virtual orbitals of 20–50 meV (a few percent of the total correlation energy). Addition of a third set of virtual orbitals to our bases would likely affect the BEs by a few meV, while approximately doubling the RCI basis size. Current coded limitations allow 20×10^3 RCI basis functions composed of up to 4×10^6 determinants, and the total number of determinantal coefficients that compose the RCI basis functions is restricted to 75×10^6. These limits could potentially be raised by added RAM or writing out data to disc, but without the approximations made in these calculations, the complexity of midrow lanthanides would require many times these current limits.

One other technique used here is to perform our calculations with the final RCI bases on anion states of higher total J, using the fact that contributions due to the second-order effects and radial basis saturation discussed above are relatively consistent for all the bound anion states of the same attachment. Recall that the number of determinants required for a given configuration of a particular J (with $M_J=J$), disregarding any j restrictions on subgroups, is equal to the number of many-electron basis functions for that configuration for its J and all possible higher J's. When dealing with a wide range of bound anion J's, as is the case in many of these calculations, the lowest J can have as much as 6–7 times the determinants as the highest J. Thus, final calculations from the higher J's are used to adjust the BEs of intermediate calculations of lower J's whenever our final bases would exceed our RCI basis size, determinant, or coefficient limits. We have previously used this approach to great effect in the case of Tc^- $4d^6 5s^2$ states [5], where RCI basis size was the limiting factor rather than determinants, and the final basis was included only in the lowest $J=0$ calculations ($\sim 10 \times 10^3$ basis functions versus $\sim 35 \times 10^3$ that would have been needed for the $J=4$ ground state).

While our RCI methodology is fully relativistic, we can perform *LS* analysis of levels by creating approximate *LS* basis functions for the configuration of interest. This process is essentially a linear transformation of the *jj* bases through simple diagonalization of the L^2 and S^2 matrices treating the major component as a nonrelativistic spinor and using the assumption that the two radial functions ($j=l\pm 1/2$) for each orbital are identical (cf. Fig. 1). We have also recently [1,2] begun performing attachment analyses in which we track the j of the neutral-core portion ($4f^m5d6s^2$) of the anion $6p$ attachments. This is particularly useful for states for which this core analysis is relatively pure, say 80% or more, since this is an indication of which photodetachment channels are most likely to be seen by experimenters. A similar analysis of anion states representing $6s$ attachments is precluded by the fact that one cannot "break" the $6s^2$ subgroup to analyze the j of the $4f^m5d^26s$ neutral-core portion of the RCI basis functions. We can, however, work backward from the neutral states, where the j of the $(m+2)$-electron subgroup, $4f^m5d^2$, indicates the J of the anion state formed when the $6s$ attachment closes the $6s^2$ ($j=0$) subgroup of the neutral threshold.

C. $4f^m$ *jls* restrictions

The largest improvement in our RCI methodology that has allowed us to tackle these midrow lanthanides is a global restriction of the *jls* of the $4f^m$ subgroup in every correlation configuration [1,2]. Throughout the lanthanide row, the $4f^{n,m}$ subgroups are quite pure (>90%) in their *ls* composition [10,18] with the dominant term having the highest allowed $s=s_d$ and the highest $l=l_d$ among terms of that s_d, as expected from Hund's rules. Secondary *ls* terms, both from our own analyses and that of experiment [10,18], consist of those with $s=s_d-1$ and $l_d-1\leqslant l\leqslant l_d+1$. For example, the dominant *ls* term of the $4f^8$ subgroup in the Tb^- calculations presented here is ^7F, and all other terms have negligible mixing except for ^5D, ^5F, and ^5G. The j of the $4f^m$ subgroup is also restricted to those allowed by the dominant term, regardless of the range of js of the secondary terms. For example, $4f^7$ in the Gd^- calculations has a dominant term of ^8S, so a single $j=7/2$ is allowed for the subgroup, despite the fact that ^6P can also make $j=3/2$ and $j=5/2$. Neutral thresholds with $4f^{n,m}$ subgroups dominated by these secondary terms typically lie much too high in the spectrum to provide significant mixing in the thresholds of interest, e.g., in Gd there are no $4f^7$ ^6P configurations among experimentally designated levels [10,18]. More details of data preparation and the combination of these $4f^m$ subgroups with the three- and four-electron valence subgroups have been presented elsewhere [1,2].

In the case of $6p$ attachments to $4f^n6s^2$ thresholds [2] determination of the mixing of the *ls* terms for each j of the $4f^n$ subgroup was straightforward due to the fact that these *ls* were the same as the total *LS* of the neutral levels with the corresponding total J, and no restriction of *ls* terms was made prior to the linear rotation (except for the case of Eu^- where restriction to ^8S and ^6P meant a great savings in determinants within the $4f^7$ subgroup). However, the presence of the $5d$ electrons in both types of attachment thresholds considered here complicates matters considerably. For example, in Tb the $4f^8$ subgroup is present with $j=6$ for $4f^85d6s^2$ $J=7/2$ through $J=17/2$ neutral levels, whereas in the prior work [2] $4f^9$ had $j=15/2$ only in the $4f^96s^2$ $J=15/2$ ground state.

For the Gd^- ($m=7$) calculations, we have actually proceeded much as in the prior case of Eu^-, since we have found a consistent ratio of ^8S to ^6P terms in the $4f^7$ subgroup of all low-lying neutral thresholds, both $4f^75d6s^2$ and $4f^75d^26s$, with the ^6P term contributing 1.95(2)% to the RCI wave function. The $4f^7$ subgroup is thus restricted to a single basis function with $j=7/2$ rotated to match this 98.05%-1.95% mixing of ^8S and ^6P, resulting in an energy loss of ~0.3 meV in a moderate sized RCI test calculation that compared this approximation to one with two pure states of ^8S and ^6P (a similar comparison in the $4f^76s^2$ level in Eu^- [2] shows less than 10 μeV difference). This rotation thus saves us a factor of two in RCI basis size, but note that the major benefit is from leaving out the other 48 basis functions of $4f^7$ $j=7/2$ that contribute ~0.02% in a much larger test calculation. Otherwise, our RCI many-electron bases would be 50 times larger, essentially impossible to attempt with this level of correlation even with a significant increase of our current memory and processing speed.

Pr^- ($m=2$) is a much simpler case, but we found a loss of ~50 meV for $4f^25d^26s$ ^6L thresholds with a similar rotation of the $4f^2$ basis. The problem was traced to different mixing of ^3H and ^1G in $4f^2$ $j=4$ and ^3H and ^1I in $j=6$ in nearby $4f^2(5d+6s)^2$ levels and even between the $^6L_{11/2}$ and $^6L_{13/2}$ thresholds. Retaining ^1G and ^1I as separate basis functions resulted in less than 1 meV change in the neutral RCI energies, so ultimately the savings in these Pr^- calculations were due to restricting the $4f^2$ j to the ^3H range (4–6) and omitting $^3F_4$, which had negligible contributions in the levels of interest, despite the experimental placement of the $4f^2(^3F)5d6s^2$ ^4H manifold ~0.4 eV [10,18] above them.

Finally, for Tb^- ($m=8$) we have relied on linear rotation within *ls* terms as a best approach to maintain similar accuracy in neutral energies in our test calculations. The dominant *ls* term of $4f^8$ is ^7F, which ranges from $j=0$ to $j=6$, and each of these j's also has at least one of the ^5G, ^5F, or ^5D secondary terms with multiplicities of 3, 2, and 3, respectively. These secondary terms contribute a few percent to the RCI wave functions, but this contribution differs by as much as several tenths of a percent between levels or between different portions of the valence subgroup, i.e., different mixing within the $4f^8$ subgroup for $4f^85d^2_{3/2}6s$, $4f^85d_{3/2}5d_{5/2}6s$, and $4f^85d^2_{5/2}6s$. Mixing of $4f^8$ within the three ^5G, two ^5F, or three ^5D functions is much more stable, however, and each of these terms is rotated to a single function, approximately halving the total size of the RCI basis with only a few meV change in the neutral energy levels. Again, the primary savings is the initial restriction to these *jls* terms. Though our $4f^8$ basis consists of 22 functions, just over 3 times the prescribed size if a single rotated function per j (0–6) were viable, the total number of possible $4f^8$ functions for this j range is over an order of magnitude larger at 228 (there are also another 67 possible $4f^8$ functions with $j>6$).

TABLE II. RCI *ab initio* BEs (meV) of Gd^- $4f^75d6s^26p$ states. Both analyses are presented as percentages (rounded, with contributions of 1% or greater). The total J of each state is given in the label of the leading LS term, and the notations of the core j in the jj analysis, (j) and $\{j\}$, indicate $6p_{1/2}$ and $6p_{3/2}$ attachments, respectively. Note the gradual flipping of the order of ^{10}F and ^8D levels from $J \leqslant 7/2$ to $J \geqslant 9/2$.

Gd^- $4f^75d6s^26p$ LS	jj attachment	BE
$^{10}F_{3/2}$ 65, ^8D 33, ^8F 1, ^6P 1	(2) 98, {3} 2	234
$^8D_{3/2}$ 67, ^{10}F 32, ^6P 1	{3} 58, {2} 40, (2) 2	78
$^{10}F_{5/2}$ 63, ^8D 33, ^8F 2, ^6P 1, ^6D 1	(3) 51, (2) 44, {4} 3, {3} 1, {2} 1	212
$^8D_{5/2}$ 52, ^{10}F 24, ^{10}D 21, ^8P 1, ^6D 1, ^6P 1	{4} 45, (3) 21, {2} 15, (2) 14, {3} 5	70
$^{10}D_{5/2}$ 74, ^8D 14, ^{10}F 10, ^8P 2	{2} 54, (2) 17, (3) 13, {3} 13, {4} 3	54
$^{10}F_{7/2}$ 60, ^8D 35, ^8F 4, ^6D 1	(3) 70, (4) 21, {5} 4, {4} 3, {3} 1	179
$^8D_{7/2}$ 59, ^{10}F 33, ^{10}D 5, ^8P 1, ^6D 1, ^{10}P 1	{5} 31, {3} 28, (4) 26, {2} 9, (3) 4, {4} 2	54
$^{10}D_{7/2}$ 90, ^{10}F 4, ^8D 5, ^8P 1	{2} 45, (4) 29, {4} 16, (3) 7, {3} 3	20
$^8D_{9/2}$ 49, ^{10}F 42, ^8F 5, ^{10}P 1, ^6F 1, ^6D 1, ^{10}D 1	(4) 82, {5} 9, {6} 5, (5) 2, {3} 1, {4} 1	135
$^{10}F_{9/2}$ 52, ^8D 44, ^{10}P 1, ^8F 1, ^6D 1, ^8P 1	{3} 33, (5) 27, {4} 17, {5} 12, {6} 11	35
$^8D_{11/2}$ 57, ^{10}F 32, ^8F 5, ^{10}P 3, ^6F 2, ^{10}D 1	(5) 73, {6} 16, (6) 5, {4} 3, {5} 5	76
$^{10}F_{11/2}$ 61, ^8D 34, ^{10}P 2, ^8F 2, ^6F 1	{4} 45, (6) 30, {6} 14, {5} 8, (5) 3	3

III. RESULTS

A. Gd^- $6p$ attachments to $4f^75d6s^2$

Binding energies for $4f^75d6s^26p$ levels of Gd^- are presented in Table II. As expected, the lesser screening of $4f^75d$ versus $4f^8$ has resulted in a larger EA than the extrapolation of the data for $4f^n6s^26p$ [2], 234 meV versus 100 meV if the ground state of Gd were $4f^86s^2$ rather than $4f^75d6s^2$. This value is in agreement with an accelerator mass spectrometry (AMS) estimate of $\geqslant$100 meV [9]. Level composition is presented using a total configurational LS basis as well as a jj attachment analysis which indicates the j of the $4f^75d6s^2$ neutral-core portion of the anion configuration where "(j)" and "$\{j\}$" denote $6p_{1/2}$ and $6p_{3/2}$ attachments, respectively. The latter analysis is useful in cases of relative purity, as it gives an indication of likely strong photodetachment channels that may be seen by experiment. For example, the lowest anion state of each $J=J_a$ (excluding $J_a=5/2$) is predominantly a $6p_{1/2}$ attachment to the neutral threshold with $J=J_a-1/2$, so a photodetachment of the form $6p \rightarrow \epsilon s+\epsilon d$ that leaves the atom in the $4f^75d6s^2$ ^9D level with $J_a=J_a+1/2$ is likely to have a relatively small partial cross section.

Despite the above examples, most of these Gd^- states have much less jj purity than the $6p$ attachments to $4f^n6s^2$ states which had typical leading terms with contributions greater than 90% [2]. An analysis of this impurity is presented graphically in Fig. 2. For comparison we have included a reproduction of the corresponding data for the six bound $4f^76s^26p$ states of Eu^- from our prior work [2]. Unlike Eu^-, the Gd^- data does not represent the final RCI anion calculations but rather a series of intermediate calculations in which we have restricted the $4f^75d6s^26p$ configuration to a specific $4f^75d6s^2$ core j and a specific $6p_{1/2}$ or $6p_{3/2}$ attachment, forcing pure jj states for this analysis. The T-shapes represent neutral thresholds with the crossbars indicating the J range of $6p$ attachments (neutral $J \pm 3/2$ with J increasing to the right) and the stems indicating the position of the neutral J's and the vertical energy scale (each stem is 200 meV). Using Eu^- as an illustration, the full circles indicate the two $6p_{1/2}$ attachments on either side of the $^8S_{7/2}$ Eu

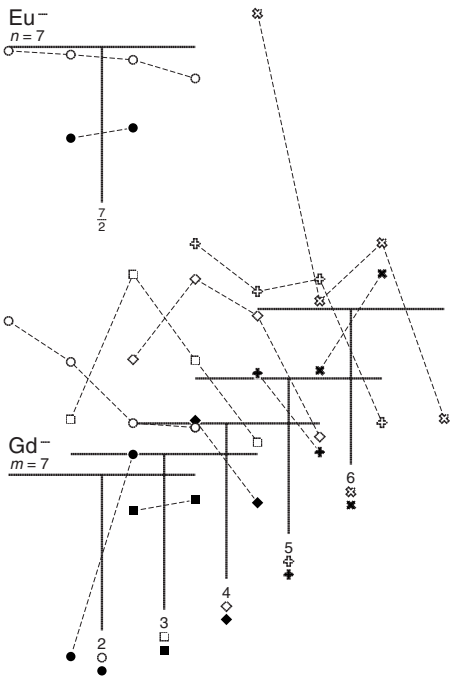

FIG. 2. Patterns of $6p$ attachments to neutral states, Eu^- $4f^76s^26p$ [2] versus Gd^- $4f^75d6s^26p$. The crossbar of the T-shaped representation of the neutral thresholds indicates the J range of $6p$ attachments (J increasing to the right), and the stem gives the position of the neutral J and the vertical energy scale (200 meV). The number at the bottom of each stem gives the neutral J and, in the Gd case, the symbols associated with that neutral level. The full and open symbols represent anion $6p_{1/2}$ and $6p_{3/2}$ attachments to those levels, respectively.

TABLE III. RCI *ab initio* BEs (meV) of Gd^- $4f^7 5d^2 6s^2$ states. Due to the high purity of these states, *LS* analyses are presented as percentages rounded to the nearest 0.1% (the total *J* of each state is given in the label of the leading *LS* term). The neutral *jj* coupling notation, $\langle j \rangle$, indicates the mixing (%) of the *j* of the $4f^7 5d^2$ subgroup. The number in parentheses in the "BE" column represents the anion binding relative to the corresponding neutral threshold from the second and third column.

Gd^- $4f^7 5d^2 6s^2$ *LS*	Gd $4f^7 5d^2 6s$ *LS*	Gd $\langle 4f^7 5d^2 \rangle 6s$ *jj*	BE
$^{10}F_{3/2}$ 97.3, ^8D 2.3, ^8F 0.4	$^{11}F_2$ 97.5, ^9D 2.1, ^9F 0.4	$\langle 3/2 \rangle$ 88, $\langle 5/2 \rangle$ 12	70(861)
$^{10}F_{5/2}$ 97.3, ^8D 1.9, ^8F 0.8	$^{11}F_3$ 97.4, ^9D 1.7, ^9F 0.8, ^9G 0.1	$\langle 5/2 \rangle$ 86, $\langle 7/2 \rangle$ 14	52(864)
$^{10}F_{7/2}$ 97.3, ^8D 1.3, ^8F 1.3, ^8G 0.1	$^{11}F_4$ 97.4, ^9D 1.2, ^9F 1.2, ^9G 0.2	$\langle 7/2 \rangle$ 87, $\langle 9/2 \rangle$ 13	26(867)
$^{10}F_{9/2}$ 97.2, ^8F 1.6, ^8D 0.8, ^8G 0.4	$^{11}F_5$ 97.3, ^9F 1.6, ^9D 0.7, ^9G 0.4	$\langle 9/2 \rangle$ 89, $\langle 11/2 \rangle$ 11	−7(874)
$^{10}F_{11/2}$ 97.4, ^8F 1.6, ^8G 0.7, ^8D 0.3	$^{11}F_6$ 97.4, ^9F 1.6, ^9G 0.7, ^9D 0.4	$\langle 11/2 \rangle$ 93, $\langle 13/2 \rangle$ 7	−51(876)
$^{10}F_{13/2}$ 97.6, ^8G 1.3, ^8F 1.1	$^{11}F_7$ 97.7, ^9G 1.3, ^9F 1.0	$\langle 13/2 \rangle$ 96, $\langle 15/2 \rangle$ 4	−97(888)
$^{10}F_{15/2}$ 97.9, ^8G 2.1	$^{11}F_8$ 97.9, ^9G 2.1	$\langle 15/2 \rangle$ 100	−148(906)

ground state; $J=3$ on the left-hand side is slightly more bound than $J=4$ on the right-hand side, 117 meV versus 104 meV [2]. The four weakly bound $6p_{3/2}$ attachments are represented by the open circles with slightly increasing BE for $J=2$ through $J=5$. The plot for Gd^- clearly shows a break in this general symmetry of the $4f^n 6s^2 6p$ data. The presence of the $5d$ electron has broken this symmetry in two ways: there is now a three-way combination of the *j*'s of the $4f^7$, $5d$, and $6p$ subgroups to make the total anion *J* (rather than the simpler $4f^n$ and $6p$ triangle inequality), and there is also different mixing of $5d_{3/2}$ and $5d_{5/2}$ in the ^9D Gd thresholds (ranging from 96% $5d_{3/2}$ in the $J=2$ ground state to 100% $5d_{5/2}$ in $J=6$), resulting in different patterns in relative attachment of the $6p$ electrons for different thresholds as seen by the dashed lines in Fig. 2.

From the analysis of Fig. 2 we can see the corresponding leading terms of the *jj* attachment analysis of Table II. The full circle to the right-hand side of the Gd ground-state stem indicates the leading "(2)" term of the Gd^- $^{10}F_{3/2}$ ground state, the two full squares correspond to the "(3)" leading terms in $^{10}F_{5/2}$ and $^{10}F_{7/2}$, and (continuing to the right-hand side in Fig. 2) the full diamond and full plus symbols similarly correspond to the "(4)" and "(5)" leading terms in $^8D_{9/2}$ and $^8D_{11/2}$. We can also gain some understanding of differences in *jj* purity of Table II from the relative positions of the pure *jj* states of Fig. 2. For example, in the $J=3/2$ case, just to the left-hand side of the Gd $J=2$ stem, we see that the "(2)" state (full circle) is over 300 meV lower than "{3}" (open square) and "{2}" (open circle), which results in a fairly pure Gd^- ground state in the final calculation. Because "{3}" and "{2}" are much closer, ~75 meV, in Fig. 2 we see much greater mixing between these states in the $^8D_{3/2}$ level. Note that additional correlation not present in these intermediate calculations and the fact that these pure *jj* states are allowed to mix in the final RCI calculations results in greater binding of this second anion state of $J=3/2$, as well as several other levels that appear above the neutral ground state in Fig. 2.

As mentioned in Sec. II B, the final energies of the lower *J*'s are determined by comparing intermediate calculations done on all *J*'s with the final energies of the higher *J*'s, where the limiting factor of the determinants is more manageable. This process necessarily assumes that our first-order calculations have accurately placed the various anion states relative to one another, ensuring very little change in the *LS* or *jj* composition from that stage to our desired final RCI bases. In this case, our coded limits could accommodate the final bases of the $J=9/2$ and $J=11/2$ calculations (two bound states for each). The increased binding between these sets of calculations is ~120 meV with a differential range among these four states of 10.0 meV. However, a linear least squared fit to these four data points based on relative composition of $6p_{1/2}$ versus $6p_{3/2}$ attachment predicts the value for each state to within 1.5 meV (essentially a pure $6p_{3/2}$ state has ~14 meV more binding at this stage than a pure $6p_{1/2}$ one). It is this linear relation that is used to scale the final values for the eight states of Table II with $J \leqslant 7/2$. To illustrate the necessity of this scaling, the final $J=9/2$ calculation has $\sim 3.5 \times 10^6$ determinants and $\sim 71 \times 10^6$ determinantal coefficients in the RCI basis functions (close to our 4×10^6 and 75×10^6 limits), and an equivalent $J=3/2$ calculation with the same valence correlation would need $\sim 12 \times 10^6$ determinants and $\sim 170 \times 10^6$ coefficients.

B. Gd^- 6*s* attachments to $4f^7 5d^2 6s$

In Table III, we present BEs for Gd^- $4f^7 5d^2 6s^2$ ^{10}F states. Note that because $S > L$ for these states as well as their $4f^7 5d^2 6s$ ^{11}F attachment thresholds, $L=3$ determines the number of possible *J*'s of each manifold, and there is a one-to-one correspondence between each of seven anion and seven neutral levels. To illustrate the point that each of these anion states appears to be a $6s$ attachment to each $4f^7 5d^2 6s$ threshold, rather than a $5d$ attachment to $4f^7 5d 6s^2$, we have also included *LS* analysis of the neutral thresholds. Note the similar mixing of each octet term in the anion levels with the corresponding nonet term in each neutral level. We have also included in the third column of Table III the neutral threshold *jj* analysis of the nine-electron $4f^7 5d^2$ subgroup as discussed in Sec. II B, which indicates that each neutral ^{11}F threshold is dominated by the configuration that would form a total *J* of the corresponding anion state of the first column when the $6s^2$ subgroup is closed.

In the course of building the bases for these Gd^- odd calculations, the process was restarted with an improved one-electron radial basis as described in Sec. II A. In this case,

TABLE IV. RCI *ab initio* BEs (meV) of Tb^- $4f^8 5d 6s^2 6p$ states. The notation has the same meaning as in Table II.

Tb^- $4f^8 5d 6s^2 6p$ *LS* (%)	*jj* attachment (%)	BE
$^9G_5$ 30, ^9F 23, ^7F 11, ^9D 11, ^9H 10, ^7G 6, ^7D 4, ^9P 3, ^7H 2	(11/2) 72, (9/2) 24, {9/2} 3, {11/2} 1	39
$^9G_6$ 35, ^9F 20, ^9H 16, ^7F 10, ^7G 9, ^9D 5, ^7H 4, ^5G 1	(11/2) 50, (13/2) 41, {11/2} 7, {15/2} 1, {13/2} 1	78
$^7F_6$ 41, ^7G 30, ^9G 13, ^9F 9, ^9D 2, ^5G 2, ^7H 2, ^9H 1	{15/2} 46, (11/2) 19, (13/2) 18, {11/2} 14, {9/2} 3	6
$^9G_7$ 37, ^9H 25, ^7G 14, ^7H 12, ^9F 11, ^9I 1	(13/2) 77, (15/2) 11, {13/2} 8, {11/2} 2, {15/2} 2	88
$^7G_7$ 52, ^9F 23, ^9G 17, ^7H 5, ^5H 2, ^9H 1	(15/2) 67, (13/2) 14, {13/2} 12, {15/2} 4, {17/2} 3	5
$^9G_8$ 46, ^9H 34, ^7H 17, ^9I 2, ^7I 1	(15/2) 74, {15/2} 15, {13/2} 10, {17/2} 1	58

anion states of lower J seemed to have more correlation contributions from $5d \rightarrow vd$ single replacement configurations, suggesting a slightly poorer zeroth-order approximation for these levels. Essentially, states with higher mixing of $5d_{3/2}^2$ in the $5d^2$ subgroup (maximum of 68% in $J=3/2$, decreasing to 0% in $J=15/2$) had problems with larger difference in $\langle r \rangle$ between the two $5d$ subshells, whereas states which were mostly $5d_{3/2}5d_{5/2}$ generated radial functions very similar to those taken from separately optimized $5d_{3/2}^2$ and $5d_{5/2}^2$ calculations. These improvements greatly decreased the range of bindings of these anion levels relative to their corresponding neutral thresholds, i.e., the spread of 15 meV in relative bindings for $J=3/2$ to $J=11/2$ was over 3 times larger (46 meV) prior to the change of radial bases.

We have included all seven states here, even though most are unbound in these *ab initio* calculations, because it is difficult to estimate the errors introduced by the many approximations made for these midrow lanthanides: $4f^m$ *jls* restrictions, careful elimination of small second-order effects, two sets of virtual orbitals only, and treatment of $4f^m$ as corelike. Most important from the analysis of Table III is that even if there is a substantial increase in the binding of these states due to a shift suggested by future experimental data, those experimenters should expect to see a single strong $6s \rightarrow \epsilon p$ feature in their spectra in the energy range of 850–950 meV, and since the true range of relative binding may be even less than presented in Table III, individual channels may be difficult to resolve.

The higher J anion states were again placed relative to the neutral $4f^7 5d^2 6s$ $J=7$ threshold which was chosen to eliminate the need to simultaneously correlate $4f^7 5d 6s^2$ ($1 \leqslant J \leqslant 6$, since $4f^7$ is restricted to $j=7/2$). In this case our limits accommodated final RCI bases for $J \geqslant 9/2$, but unlike the $6p$ attachments, the final increases in correlation were consistent to within 1 meV for all the higher J anion levels, so a common amount was used to scale energies of the lower J's. A $J=3/2$ calculation with this final RCI basis would have required $\sim 9 \times 10^6$ determinants and $\sim 125 \times 10^6$ coefficients.

C. Tb^- $6p$ attachments to $4f^8 5d 6s^2$

In Table IV we present BEs for Tb^- $4f^8 5d 6s^2 6p$ states, $6p$ attachments to the low-lying Tb $4f^8 5d 6s^2$ ^8G thresholds that begin just 35 meV [10,18] above the $4f^9 6s^2$ ground state. The prior study of $6p$ attachments to $4f^m 6s^2$ ground states [2] produced a maximum BE of 85 meV relative to $4f^9 6s^2$ $^6H_{15/2}$. Here the $4f^8 5d 6s^2 6p$ $^9G_7$ state is bound relative to $4f^8 5d 6s^2$ $^8G_{13/2}$ by 123 meV, indicating a slightly reduced screening of the nuclear charge by $4f^8 5d$ relative to $4f^9$. Given the approximations and difficulties of these calculations and the 3 meV difference in BE relative to the ground state, it seems too close to call for these RCI calculations, but the BE of 88 meV from Table IV certainly suggests that the ground state of the Tb^- anion may be an attachment to the neutral Tb first excited state.

While our Tb^- EA is below the AMS value of $\geqslant 100$ meV [9], increased anion binding is certainly possible given the approximations required to perform these calculations, including the increased difficulty of *jls* restrictions of $4f^8$ compared to $4f^7$ in Gd^- as discussed in Sec. II C. Our principle goal here is to provide a reasonable identification of anion levels, both in terms of leading *LS* terms and relative position, to assist in analysis of experimental spectra. More recent LPES measurements [19] suggest an EA for Tb^- >1.165 eV, but our expectation is that such experiments are likely to see strong features in photodetachment spectra representing channels that leave the neutral atom in excited-state thresholds, and that studies using appropriate incident photon energies should be able to exploit these channels. For example, given the near degeneracy of $4f^9 6s^2 6p$ and $4f^8 5d 6s^2 6p$ in these calculations, one would hope to find a photodetachment threshold that would help distinguish the two types of attachments. If we consider $6s \rightarrow \epsilon p$ in both cases, we can see from Table I that there is also a near degeneracy, 1.846 eV versus 1.860 eV [10,18], in the lowest-lying $4f^9 6s 6p$ and $4f^8 5d 6s 6p$ thresholds, suggesting possible difficulties in resolving these channels in experimental data. However, if we consider $5d \rightarrow \epsilon p + \epsilon f$ photodetachment from the odd states (likely a smaller cross section given the smaller $\langle r \rangle$ of $5d$ versus $6s$), we note from Table I that $4f^8 6s^2 6p$ thresholds beginning at 1.688 eV [10,18] should be separated enough from the above manifolds to identify a feature in the data at the appropriate energy.

These Tb^- odd calculations represent the most difficult calculations in our lanthanide studies. As mentioned in the prior $4f^m 6s^2 6p$ study [2], Sm^- ($n=6$) was actually more difficult than Eu^- ($n=7$) due to the fact that the Eu^- $4f^7$ subgroup (with an ^8S dominant term) was restricted to a single $j=7/2$. A similar situation exists here between Tb^- and Gd^-, since our prescription of our $4f^m$ *jls* restrictions retains all seven j's of the ^7F term (with our anion states of interest having total $J \geqslant 5$, potential omission of the bottom few $j=0,1,2$ of this subgroup would actually affect RCI basis sizes by only a few percent). While our final RCI bases of

~6000 functions for Gd^- were well within the coded 20×10^3 limit, these Tb^- calculations were constrained by this limit as well as the 4×10^6 determinant and 75×10^6 coefficient limits. In order to approximate the same level of correlation as presented in the Gd^- $6p$ attachments of Table II the final RCI basis had to be moderately trimmed to create a $J=8$ calculation that fit within these constraints, and a final estimate of the remainder was made by an unbound $J=9$ calculation. Scaling for $J\leqslant7$ was performed in a similar manner as the Gd^- case as discussed in Sec. III A. A hypothetical $J=5$ calculation made with the equivalent RCI basis would contain over 100×10^3 basis functions consisting of $\sim15\times10^6$ determinants and nearly $\sim5\times10^9$ coefficients. More importantly, comparing to the run times on our 2.5 GHz PC, this $J=5$ calculation would take about 2 months of CPU time versus a typical 1 day of computation time for the largest calculations of this study. Again, the above comments are disregarding the basis size reduction by an order of magnitude from our $4f^8$ subgroup *jls* restrictions, without which calculations with a tiny fraction of the correlation included here would be prohibitively expensive, and the above hypothetical $J=5$ calculation would be pushed into a time frame of several years.

D. Pr^- $6s$ attachment to $4f^25d^26s$

Our previous lanthanide study [2] predicted a Pr^- $4f^36s^26p$ ground state with an EA of 177 meV, consistent with an AMS estimate of $\geqslant100$ meV [9]. Therefore, our proposed $6s$ attachment to the excited $4f^25d^26s$ $^6L_{11/2}$ threshold at 0.832 eV [10,18] would be an excited anion level. Note that our neutral calculation for $J=11/2$ was performed using one-electron radial functions and virtual orbital Z^*'s optimized to the $^6L_{11/2}$ level. Our usual approach of using a higher J threshold, 19/2 in this case, to eliminate the need to simultaneously correlate $4f^25d6s^2$ was precluded by the fact that energies of the $4f^25d^26s$ ^6L manifold are not known experimentally [10,18] for $J\geqslant15/2$.

This $6s$ attachment was determined to be unbound by the earlier calculations of our group [25], but improvements of our anion one-electron radial basis have increased the relative binding enough to predict a single weakly bound $J=6$ state with a BE of 24 meV. The importance of this state is apparent when we consider the LPES measurements of Davis and Thompson [26] which found two peaks in the photoelectron kinetic energy spectrum with transition energies of 0.962(24) eV and 0.866(18) eV using an incident photon energy of 1.165 eV. From Table I we see that the $4f^36s6p$ thresholds begin at 1.665 eV [10,18], so $6s\rightarrow\epsilon p$ photodetachments from the even anion states could not be seen by this experiment. However, given the separation of the two peaks, 96 meV, and the error bars on the measurements, the 114 meV difference between the $^6L_{11/2}$ and $^6L_{13/2}$ thresholds seems to be the best candidate to explain these features of the photodetachment spectrum. If we split the difference by subtracting the average of the two experimental peaks, 914 meV, from the average of the two threshold energies, 889 meV, we get a BE relative to the Pr ground state of 25 meV, in excellent agreement with our calculation.

The LS composition of our single bound state is 92% $^5L_6$ with 8% mixing of ^3K. Unlike the Gd case presented in Sec. III B, with $L>S$ there is one fewer potential anion state in the ^5L manifold than in the ^6L neutral manifold, so the one-to-one correspondence of anion and neutral states found in Gd is not seen here. In fact, the analysis of the $4f^25d^2$ subgroup in our neutral calculations showed 99.9% purity of $j=6$ for the $^6L_{11/2}$ threshold, but nearly equal mixing, 55% to 45%, of $j=7$ and $j=6$ in the $^6L_{13/2}$ threshold. This suggests that our $^5L_6$ anion state would have large photodetachment cross sections via $6s\rightarrow\epsilon p$ to both of these thresholds, and we note that the larger peak in the experimental kinetic energy spectrum [26] is the one with higher photoelectron energy, which would correspond to the lower (and more pure $j=6$) $^6L_{11/2}$ level.

Given the approximations and difficulties that have gone into these calculations, even with small $m=2$ for Pr^-, the placement of our bound state within 1 meV of the expected target seems incredibly fortuitous. Our confidence in this position, however, lies in the threshold analysis mentioned above. An RCI anion calculation of the $^5L_7$ level was found to lie ~130 meV above the $^5L_6$ level, unbound by over one-tenth of an eV relative to the neutral ground state. Note that this separation is also similar to the experimental difference of 96 meV [26], in fact barely within range if one stretches the error bars in opposite directions (138 meV maximum). One might consider that additional binding of ~100 meV of the anion states might also explain the two experimental peaks as two anion states detaching to a single neutral threshold rather than a single bound state detaching to two thresholds. However, if this were the case the two channels of $^5L_6\rightarrow{}^6L_{11/2}+\epsilon p$ and $^5L_7\rightarrow{}^6L_{13/2}+\epsilon p$ might have transition energies similar to the 0.962 eV peak of the experiment [26], but the corresponding $^5L_7\rightarrow{}^6L_{11/2}+\epsilon p$ channel would not create the noticeable 0.866 eV peak [26] since there is no $4f^25s^2$ $j=7$ mixing in the $J=11/2$ threshold, and there would instead be a second peak with transition energy of ~1.075 meV from the $^5L_6\rightarrow{}^6L_{13/2}+\epsilon p$ channel.

Given the results of these two studies, we suggest to interested LPES or LPTS experimenters that photon energies in the range of 1.8 eV to 2.0 eV or higher would be useful in identification of channels involving the predicted Pr^- ground state [2,25], i.e., $4f^36s^26p\rightarrow4f^36s6p+\epsilon p$ (0.177 eV [2] +1.665 eV [10,18]).

E. Review and update of Lu^- $m=14$ states

To complete this lanthanide survey, we have revised our earlier work on the ends of the lanthanide row. Since the relative simplicity of these systems has historically resulted in more computational interest, we also provide here a brief review of each of these anion cases.

Vosko and Chevary [27], using Dirac-Hartree-Fock (DHF) and density functional theory (DFT), predicted a ground state of Lu^- via $6p$ attachment to the Lu $5d6s^2$ ground state with an EA of 190(110) meV, contrary to the then expected $5d$ (or $4f$) attachment. From Table I we see that Lu $5d^26s$ levels begin at 2.337 eV [10,18], so this is not unexpected when considering $5d^26s^2$ as a $6s$ attachment to

TABLE V. RCI BEs (meV) of Lu^- $6p$ attachments, both even ($6s^26p^2$) and odd ($5d6s^26p$) parity. The notation has the same meaning as in Table II. Values in the "$4f^m$ BE" column are from calculations with correlation equivalent to the Gd^- and Tb^- $6p$ attachments presented in Tables II and IV. The "BE" column contains the recommended RCI values of our "complete" calculations as discussed in Sec. III E.

Lu^- $6s^26p^2/5d6s^26p$ *LS* (%)	*jj* attachment (%)	BE	$4f^m$ BE	Earlier BE [15]
$^3P_0^e$ 94, ^1S 6	(1/2) 86, {3/2} 14	78		
$^1D_2^o$ 68, ^3F 30, ^3P 1, ^3D 1	(3/2) 77, {5/2} 12, {3/2} 6, (5/2) 5	353	308	329
$^3F_2^o$ 70, ^1D 29, ^3P 1	{3/2} 39, (3/2) 20, {5/2} 20, (5/2) 19	154	102	124
$^3F_3^o$ 99, ^3D 1	{3/2} 50, (5/2) 50	96	39	63

these thresholds. Eliav *et al.* [21], using the relativistic Fock-space coupled-cluster method, confirmed this ground-state configuration with an EA of 260 meV and also predicted an opposite parity $6s^26p^2$ state bound by 93 meV. The AMS EA from the anion survey of Nadeau *et al.* [9] was $\geqslant$100 meV, consistent with these calculations. Our earlier RCI calculations [15] then predicted three Lu^- $5d6s^26p$ bound states as shown in Table V, increasing the EA prediction to 329 meV. The LPES measurements of Davis and Thompson [17] yielded two bound states with binding energies of 340(10) meV and 160(20) meV. Finally, recent Regge-pole calculations of Felfli *et al.* [28] have produced a much smaller EA of 29 meV.

Note that the "$4f^m$ BE" column in Table V includes valence correlation equivalent to the Gd^- and Tb^- $6p$ attachments. The difference between these values and our original RCI BEs [15] is accounted for by inclusion of several more second-order effects (~10 meV), a third set of virtuals (also ~10 meV), and vg orbitals (2–3 meV); all of which are omitted in the Gd^- and Tb^- calculations as they would otherwise more than double our RCI bases. The differences between these limited bases and the highest BEs presented in Table V are a good indication of possible increased binding that may be missing from the Gd^- and Tb^- calculations. Given the relative simplicity of these calculations, we have the luxury of including essentially every possible four-electron correlation configuration that might contribute to the anion energies (and corresponding correlation in the three-electron neutral calculations where applicable). These "complete" calculations contain RCI bases approximately 5 times larger than the "$4f^m$" calculations, including two sets of virtual orbitals up to vh in the first and vf' in the second. Correlation is included for configurations representing all combinations of the $5d$, $6s$, and $6p$ DF orbitals for each parity as well as second-order correlation that contains three or four virtual subshells. We note, however, that relative position of anion states and their composition is relatively stable (with ~10 meV) in these final stages of the calculations, which has been our principle assumption in the mid-row calculations of this survey [2].

Interestingly, the inadequacies of our one-electron radial bases were noted in our earlier study [15], and a separate series of $J=2$ calculations were made with radial functions and virtual orbital Z^*'s optimized to the second level. This separate treatment of $^3F_2$ can be seen in the *LS* analysis of the earlier work where, for example, the single ^3F basis function appears to contribute 114% total to the two states (impossible within a single calculation). In the "$4f^m$" values here we have improved the one-electron radial basis with our hybrid $6p$ subshell and arrived at the same splitting of the $J=2$ levels to within 1 meV in a single calculation. While the EA presented here has actually surpassed the experimental error bars, we note that 353 meV and 154 meV are together in better agreement with the experimental values [17]. These two experimental values were originally identified with the $^1D_2^o$ ground state and the $^3P_0^e$ state predicted by Eliav *et al.* [21]. We disagree with the second identification because that analysis relied on identifying peaks corresponding to detachments to the Lu $^2D_{3/2}$ ground state, and a photodetachment of the form $6s^26p^2 \rightarrow 5d6s^2+\epsilon p$ is unlikely without considerable mixing of $5d^26s^2$ in this anion state.

Assuming the two experimental BEs correspond to the two $J=2$ levels, we checked for possible features in the experimental spectrum [17] that could correspond to the other two predicted levels but found that these channels were likely unresolved from those with $J=2$ initial states. Since the $^3P_0^e$ level is primarily $6s^26p_{1/2}^2$, the $6s^26p_{1/2}$ threshold is the only likely candidate for a strong photodetachment channel with an expected photoelectron kinetic energy close to the peak labeled "4" in the spectrum of Fig. 1 of Ref. [17], i.e., possibly degenerate with the $^1D_2^o \rightarrow {}^2D_{5/2}+(\epsilon s+\epsilon d)$ channel. Similarly, we note detachments from $^3F_3^o$ to $^2D_{3/2}$, $^2D_{5/2}$, $^2P_{1/2}$, and $^2P_{3/2}$ could also contribute to the experimental peaks labeled ",1" "2," "5," and "7" [17].

F. Review and update of La^- $m=0$ states

While, La and Lu have essentially the same valence configurations, the difference being the closed $4f^{14}$ subgroup in Lu, we can see from Table I that the low-lying $5d^26s$ manifolds of La starting at 0.331 eV [10,18] allow for La^- $5d^26s^2$ anion states, while none are present in Lu^-. Vosko *et al.* [29] confirmed this uniqueness of La^- within the group IIIB anions with DFT-HF calculations that predicted a $5d^26s^2$ ^3F state bound by 110–270 meV and identified the reason for this dissimilarity with Sc, Y, and Ac (see Sec. I) as this low-lying La $5d^26s$ configuration. These calculations also predicted three $5d6s^26p$ bound anion states: ^1D, ^3D, and ^3F with BEs in the ranges of 270–410 meV, 140–220 meV, and 110–220 meV, respectively.

The experimental AMS measurements of Nadeau *et al.* [9] predicted an EA >500 meV, in apparent agreement with the semiempirical extrapolation of the third transition series linear trend [8] (~0.84 eV bound relative to $5d^26s$ at 0.331 eV). LPES measurements of Covington *et al.* [16] identified two bound states with BEs of 470(20) meV and

TABLE VI. RCI BEs (meV) of La^- $5d6s^26p$ states. The notation has the same meaning as in Table II. Values in the "$4f^m$ BE" column are from calculations with correlation equivalent to the Gd^- and Tb^- $6p$ attachments presented in Tables II and IV. The "BE" column contains the recommended RCI values of our "complete" calculations as discussed in Sec. III E.

La^- $5d6s^26p$ *LS* (%)	*jj* attachment (%)	BE	$4f^m$ BE	Earlier BE [14]
$^3P_0$ 100	{3/2} 100	10	−43	
$^3D_1$ 99, ^1P 1	(3/2) 59, {3/2} 34, {5/2} 7	208	162	235
$^1D_2$ 82, ^3F 16, ^3D 1, ^3P 1	(3/2) 62, {5/2} 20, {3/2} 12, (5/2) 6	434	404	462
$^3F_2$ 82, ^1D 17, ^3P	{3/2} 37, (3/2) 34, {5/2} 17, (5/2) 12	286	248	282
$^3D_2$ 98, ^1D 1, ^3P 1	{3/2} 46, (5/2) 44, {5/2} 9, (3/2) 1	149	104	145
$^3F_3$ 99, ^3D 1	{3/2} 52, (5/2) 48	240	199	247
$^3D_3$ 98, ^1F 1, ^3F 1	{5/2} 64, (5/2) 21, {3/2} 15	84	36	56
$^3F_4$ 100	{5/2} 100	139	96	84

170(20) meV. Our initial RCI calculations for La^- [14] made extensive use of second-order correlation and core-valence correlation involving the $5p$ subshell, and results seemed to corroborate the LPES values by identifying the two experimental values with two $5d6s^26p$ levels with BEs of 462 meV and 235 meV (see Table VI). The $5d^26s^2$ states in these calculations were found to be slightly less bound with their highest BE of 434 meV (see Table VII).

In revisiting La^- here we have left the core closed, given the absence of core-valence correlation in the rest of this lanthanide survey [2]. Opening the core can cause problems with unintentional over-correlation of one configuration over another, which may have been the case in the earlier work [14]. Large energy contributions from $5p^2$ double replacements on the order of 1 eV or more, essentially doubling the RCI correlation energy, can drastically alter the relative position of levels of some valence correlation configurations relative to levels of interest. In the earlier RCI study, we had attempted to alleviate this problem by partially opening the $5p$ subshell with exclusion-type correlation only, i.e., configurations involving subshells with differing occupation between the neutral attachment thresholds and anion states. For example, in the odd $6p$ attachments $5p6p$ pair correlation and double replacements of the form $5p^2 \rightarrow p^2$ were included, while $5p5d$ and $5p6s$ pair correlation and $5p^2 \rightarrow s^2 + sd$ double replacements were added to the even calculations. A review of the correlation tables [14], however, shows that these same types of replacements were not included in all the important valence configurations as a proper treatment of second-order correlation would require.

TABLE VII. RCI BEs (meV) of La^- $5d^26s^2$ states. Values in the "$4f^m$ BE" column are from calculations with correlation equivalent to the Gd^- $6s$ attachments presented in Table III and the Pr^- calculation discussed in Sec. III D. The "BE" column contains the recommended RCI values of our "complete" calculations as discussed in Sec. III E. Note that these more recent calculations indicate this $^3F_2^e$ level is the La^- ground state, contrary to our earlier study [14] which had $^1D_2^o$ more bound.

La^- $5d^26s^2$ *LS* (%)	BE	$4f^m$ BE	Earlier BE [14]
$^3P_0$ 98, ^1S 2	128	27	
$^3P_1$ 100	103	5	
$^3F_2$ 96, ^1D 3, ^3P 1	545	478	434
$^1D_2$ 90, ^3P 6, ^3F 4	259	118	62
$^3P_2$ 93, ^1D 7	52	−61	
$^3F_3$ 100	478	412	375
$^3F_4$ 100	410	340	312

The first set of BE values in Table VI represents the "complete" calculation with the equivalent correlation as described in the Lu^- case in Sec. III E, i.e., all possible second-order effects, inclusion of vg and vh, etc. Our interpretation of the similarity of these final BEs with those of the earlier calculations is that, much like single replacements of the same symmetry, some of the core-valence contribution in the earlier calculations (specifically, $5p6p \rightarrow vp^2 + vpvp'$) actually represented corrections to the inadequate $6p$ one-electron radial functions. The improvements in treatment of $6p_{3/2}$ attachments is evident in the fact that while the two $6p_{1/2}$ attachments are less bound by 27 meV and 28 meV, most of the $6p_{3/2}$ attachments are more bound in these final calculations than in the earlier work [14].

Increased binding of the recent calculations in the even anion states of Table VII, even in the "$4f^m$" values despite removal of the $5p$ correlation, is similarly due to improvements in the one-electron $5d$ radial functions. These improvements combined with the slight decrease in the lowest odd BE have caused the RCI identification of the ground-state configuration to flip to $5d^26s^2$. Diffuse $5d_{3/2}$ and $5d_{5/2}$ functions were purposely selected, but the initial MCDF calculations were also improved by inclusion of a DF $6p$ orbital even though none is present in either $5d^26s$ or $5d^26s^2$. The inclusion of $5d6s \rightarrow 6p^2$ and $6s^2 \rightarrow 6p^2$ replacements in these calculations results in greater mixing of $5d_{3/2}5d_{5/2}6s^2$ in the MCDF-stage anion states, where nearly pure $5d_{3/2}^2 6s^2$ states in the earlier work created a $5d$ subshell that was less suitable to zeroth-order approximation of excited anion levels.

Note that, ironically, the "$4f^m$" EA of Table VII actually agrees quite well with the Covington *et al.* 470(20) eV EA [16]. In fact, their experimental analysis relied on a peak in the photoelectron kinetic energy spectrum that was identified essentially as the centroid of the anion ground state to the two neutral $5d6s^2$ levels, $^2D_{3/2}$ (ground state) and $^2D_{5/2}$ (131 meV [10,18]). However, our RCI calculations show that

the $^3F_2$ ground state is 83% pure $5d_{3/2}^2 6s^2$, suggesting a strong $5d_{3/2} \rightarrow \epsilon p + \epsilon f$ photodetachment only to the neutral ground-state channel. Accounting for this point by shifting the experimental spectrum's analysis [16] by 65 meV, approximately one-half the energy difference of the ^2D thresholds, to 535(20) meV results in much better agreement with our final RCI EA of 545 meV. This shift would also result in closer alignment of other peaks in the experimental spectrum [16] with $6s \rightarrow \epsilon p$ photodetachment channels from the La^- $5d^2 6s^2$ $^3F_2$ ground state to neutral $5d^2 6s$ $^4F_{3/2}$, $^4F_{5/2}$, and $^2F_{5/2}$ thresholds at 331 meV, 373 meV, and 869 meV, respectively. Much as in our interpretation of the many bound states in Ce^- [7] with same *LS* terms but different *J*'s, similar energy differences occur for the higher *J* anion ^3F levels detaching to higher *J* ^4F and ^2F neutral thresholds. Finally, while there is no definitive identification of each of the remaining peaks of the experimental spectrum, we suggest that some odd levels, particularly the ^3F ones, are in reasonable positions to detach via $6p \rightarrow \epsilon s + \epsilon d$ to $5d6s^2$ and via $6s \rightarrow \epsilon p$ to $5d6s6p$ thresholds starting at 1.644 eV [10,18] to explain some of these features (as originally suggested in the experimental analysis [16]).

G. Review and update of Ce^- $m=1$ states

Ce^- is perhaps the most interesting and most difficult lanthanide anion from the computational perspective. While the complexity of RCI basis functions with $m=1$ is much less than $m=7$ in Gd and $m=8$ in Tb, difficulties arise from the density of low-lying states in the Ce neutral spectrum. Consider, for example, the position of the lowest $4f^m 5d^2 6s$ thresholds [10,18] for the lanthanides of this study and then note the number of nearby states above these thresholds, whose relative positions may be critical for proper mixing of the $4f^m 5d^2 6s$ states of interest. For Ce $J=2,3,4$ there are 19, 14, and 13 levels within 1 eV of the lowest $4f5d^2 6s$ state. For Pr^- the count is slightly fewer with nine and 12 additional levels within 1 eV of $4f^2 5d^2 6s$ $J=11/2$ and $J=13/2$ (recall it was problems with mixing of these levels that led us to retain $4f^2$ ^1G and ^1I basis functions as discussed in Sec. II C). Moving across the row, however, when one reaches Gd there are at most two or three levels within 1 eV of the lowest $4f^7 5d^2 6s$ threshold regardless of *J*, which is the same count as the two or three levels within 1 eV of $5d^2 6s$ ^4F thresholds in La. Combined with the fact that the lowest $4f5d^2 6s$ manifold in Ce begins at just 0.294 eV [10,18], there are a wealth of potential 6*s* attachment thresholds over a wide range of *J*'s.

In the early 1990s high yields of Ce^- AMS studies by Berkovits *et al.* [30] and Garwan *et al.* [31] suggested a large EA, perhaps >600 meV. The initial RCI calculation of our group [3] predicted several $4f5d6s^2 6p$ levels with an EA of 259 meV and a single $4f5d^2 6s^2$ state bound by 179 meV. Later AMS studies essentially confirmed the earlier experimental estimates with Nadeau *et al.* [9] giving an EA value of ⩾500 meV and Berkovits *et al.* [32] increasing this value to 700(10) meV, though the latter was dependent on the earlier RCI ground-state identification.

Our first revisit of our Ce^- RCI calculations [33] flipped the identity of the ground state with a $4f5d^2 6s^2$ EA of 428 meV and highest $5d6s^2 6p$ BE of 349 meV. A later LPES study of Davis and Thompson [13] identified at least three bound states with BEs of 955(26) meV, 921(25) meV, and 819(27) meV. Cao and Dolg [6], using the relativistic energy-consistent small-core pseudopotential methodology, also predicted a $4f5d^2 6s^2$ Ce^- ground state now with an EA of 530 meV, leaving a discrepancy of 425 meV between the most recent experiment and calculation at the time.

We again revisited our RCI Ce^- calculations in Ref. [7], this time performing a detailed study of photodetachment partial cross sections, which suggested that the ground-state to ground-state channel ($5d \rightarrow \epsilon p + \epsilon f$) was much weaker than channels to $4f5d^2 6s$ ^5H thresholds ($6s \rightarrow \epsilon p$). This reinterpretation of the experimental spectra effectively lowered the measured EA to ~660 meV, but our *ab initio* EA was only 511 meV, in good agreement with Cao and Dolg [6] but still ~150 meV lower than experiment. However, our highest *ab initio* $4f5d6s^2 6p$ BE was 328 meV, in reasonable agreement with the 300 meV value determined by this reinterpretation. Because we now regard Ce^- as the model case for melding computational [7] and experimental [13,20] analysis in these photodetachment studies, we have presented all BEs in Tables VIII and IX adjusted to these values.

An LPTS study by Walter *et al.* [20] that focused on the incident photon energy range of 610–750 meV found a *p*-wave threshold above ~650 meV, which is consistent with the ground-state to ground-state channel of the reinterpretation of the Davis and Thompson spectra [13]. Finally, recent Regge-pole calculations of Felfli *et al.* [34] have predicted a Ce^- EA of 610 meV, in much closer agreement with our RCI values than in the Lu^- case [28].

Much as in the case of the La^- $5p$ correlation, we have found in our recent *ab initio* calculations that improvements of one-electron radial functions have made the correlation involving the $4f$ electron in the earlier calations [7] obsolete. That is, prior to our semiempirical adjustment of the $6p$ attachment BEs to match the expected 300 meV value of the $^2H^e_{9/2}$ BE, this state was bound by 326 meV compared to 328 meV in the earlier calculation. Similarly, the $^4H^o_{7/2}$ Ce^- ground state is bound by 530 meV compared to 511 meV in the earlier calculation prior to the adjustment to match the 660 meV EA. Test calculations designed to check correlation involving the $4f$ electron using the improved one-electron bases showed that replacements "out of $4f$" (configurations with no $4f$ electrons) as well as "into $4f$" (configurations with $4f^2$ or $4f^3$ subgroups) both contributed ~100 meV to RCI energies, but the differential contribution between anion and neutral calculations was ~2 meV, resulting in negligible impact on BEs. Of course, the question remains as to what is missing from the 6*s* attachment calculations to bridge the remaining 130 meV gap between our adjusted EA and the calculation with RCI bases equivalent to our Gd^- 6*s* attachments. Similar to the La^- and Lu^- cases, we found that the EA could be somewhat improved by inclusion of additional second-order effects and configurations with *vg* virtuals, providing an additional binding of ~35 meV.

Considering the density of states as discussed above, we have found that proper positioning of higher $4f5d^2 6s$ and $4f5d^2 6s^2$ levels is more critical in Ce and Ce^- than in La^- or Gd^-. We note that our lowest anion $6p$ attachments are being

TABLE VIII. RCI *ab initio* BEs (meV) of Ce^- $4f5d6s^26p$ states calculated relative to the lowest $6p$ attachment, which has been placed at 300 meV to match the experimental data [13] and our earlier interpretation of these data [7]. The notation in the first two columns has the same meaning as in Table II. The third column core *ls* analysis (%) is included to illustrate the bound states that are actually attachments to low-lying ^3F and ^3H manifolds [10,18].

Ce^- $4f5d6s^26p$ *LS*	*jj* attachment	Core $^1G\|^3F\|^3H$	BE	Earlier BE [7]
$^2D_{3/2}$ 62, ^4F 25, ^4D 7, ^2P 6	(2) 88, (1) 3, {3} 3, {1} 3, {0} 2, {2} 1	0|84|0	95	141
$^2F_{5/2}$ 48, ^4G 47, ^2D 5	(2) 68, {4} 25, (3) 3, {2} 3, {1} 1	18|55|4	152	156
$^4G_{5/2}$ 47, ^2F 41, ^2D 11, ^4F 1	{4} 38, (2) 25, {2} 21, (3) 9, {3} 5, {1} 2	31|57|0	1	
$^4G_{7/2}$ 87, ^4H 8, ^2F 2, ^4F 2, ^4G 1	{4} 51, (4) 24, {2} 15, {5} 4, (3) 3, {3} 3	55|23|18	179	185
$^4H_{7/2}$ 37, ^2F 27, ^2G 27, ^4G 8, ^4D 1	(4) 65, {2} 13, {4} 10, (3) 9, {3} 2, {5} 1	25|12|48	104	83
$^2F_{7/2}$ 41, ^4H 35, ^4G 13, ^2G 8, ^4D 2, ^4F 1	(4) 51, {4} 28, (3) 15, {2} 5, {3} 1	28|18|37	28	
$^2H_{9/2}$ 67, ^2G 17, ^4I 12, ^4H 3, ^4G 1	(4) 84, {4} 10, {5} 4, (5) 1, {3} 1	38|3|57	300	300
$^4I_{9/2}$ 47, ^2G 43, ^4F 4, ^4H 3, ^2H 2, ^4G 1	{4} 60, (4) 37, {3} 2, {6} 1	41|6|52	98	45
$^2H_{9/2}$ 40, ^2G 30, ^4I 23, ^4F 4, ^4H 2, ^4G 1	{4} 68, (4) 14, {5} 11, {3} 4, (5) 2, {6} 1	26|7|61	18	
$^2H_{11/2}$ 70, ^4I 23, ^4G 4, ^4H 2, ^2I 1	{4} 67, (5) 25, {6} 4, {5} 2, (6) 2	52|4|43	78	76

compared to their natural threshold, the $4f5d6s^2$ $^1G_4$ ground state, so any problems that occur due to positioning of nearby states is somewhat alleviated, i.e., the density of states in the anion $J=7/2$ and $J=9/2$ calculations is similar to the neutral $J=4$ reference calculation, resulting in reasonable agreement with our expected largest BE of 300 meV [7]. In the $6s$ attachments, however, our selected neutral reference level, $4f5d^26s$ $^5I_7$ (chosen since $4f5d6s^2$ can only make $J\leqslant 6$), has just three more neutral thresholds within 1 eV of its position, whereas the lowest $4f5d^26s$ $^5H_3$ and $^5H_4$ attachment thresholds have counts of 14 and 13 levels within 1 eV as mentioned above. To verify that this difference in

TABLE IX. RCI BEs (meV) and *LS* composition (%) of Ce^- $4f5d^26s^2$ states. The *ls* analysis (%) for mixing of terms in the $5d^2$ electron subgroup is presented to illustrate the relative improvements in states with less ^3F purity. Binding energies are presented for the *ab initio* and shifted calculations discussed in Sec. III G as well as the most recent previous values of our group [7]. All three sets of data are presented relative to the Ce^- $^4H_{7/2}$ ground state which is placed at 660 meV to match the experimental data [13]. Please note the typographical error in our earlier *LS* analysis [7] that incorrectly identified the secondary term of the Ce^- $^4H_{7/2}$ ground state as ^4G rather than ^2G.

Ce^- $4f5d^26s^2$ *LS*	$5d^2$ subgroup *ls*	BE	Shifted BE	Earlier BE [7]
$^4D_{1/2}$ 77, ^2P 20, ^2S 1	^3F 66, ^3P 20, ^1D 12	349	396	302
$^2S_{1/2}$ 40, ^2P 28, ^4P 18, ^4D 14	^3F 75, ^1D 20, ^3P 5	134	198	73
$^4D_{3/2}$ 92, ^2P 28, ^4P 18, ^4D 14	^3F 70, ^1D 20, ^3P 5	281	305	231
$^4F_{3/2}$ 94, ^2D 5, ^4D 1	^3F 86, ^3P 12, ^1D 2	108	125	106
$^2F_{5/2}$ 65, ^4D 27, ^4G 4, ^4F 3, ^2D 1	^3F 63, ^1D 17, ^3P 15, ^1G 3, ^1S 2	292	349	234
$^4D_{5/2}$ 65, ^2F 24, ^4G 7, ^2D 3, ^4F 1	^3F 66, ^3P 25, ^1D 7, ^1G 1, ^1S 1	180	220	125
$^4G_{5/2}$ 54, ^4F 37, ^2F 4, ^4D 3, ^2D 2	^3F 86, ^3P 10, ^1D 3, ^1G 1	70	84	54
$^4F_{5/2}$ 56, ^4G 31, ^2F 11, ^2D 2	^3F 81, ^3P 9, ^1D 9, ^1G 1	19	42	
$^4H_{7/2}$ 73, ^2G 26, ^2F 1	^3F 94, ^1D 3, ^3P 2, ^1G 1	660	660	660
$^2G_{7/2}$ 56, ^4H 26, ^2F 15, ^4G 2, ^4D 1	^3F 80, ^3P 10, ^1D 7, ^1G 3	431	456	428
$^2F_{7/2}$ 45, 4D 32, ^2G 16, ^4F 6, ^4H 1	^3F 70, ^3P 18	253	290	232
$^4D_{7/2}$ 38, ^2G 28, ^4G 23, ^2F 10, ^4F 1	^3F 51, ^3P 29, ^1D 20	47	153	8
$^4H_{9/2}$ 64, ^2G 31, ^2H 4, ^4F 1	^3F 92, ^3P 5, ^1D 2, ^1G 1	560	562	550
$^4I_{9/2}$ 92, ^2H 6, ^4H 2	^3F 96, ^1D 4	516	513	508
$^2G_{9/2}$ 61, ^4H 34, ^4F 2, ^4G 2, ^4I 1	^3F 85, ^3P 13, ^1G 1, ^1D 1	413	420	403
$^2H_{9/2}$ 84, ^4I 7, ^2G 6, ^4H 2, ^4G 1	^1D 62, ^3F 33, ^1G 4, ^3P 1	166	296	126
$^4H_{11/2}$ 50, ^4I 45, ^2I 5	^3F 98, ^1G 2	423	414	419
$^4I_{11/2}$ 48, ^4H 46, ^2H 5, ^2I 1	^3F 98, ^1D 2	383	374	380
$^2I_{11/2}$ 91, ^4I 5, ^2H 3, ^4H 1	^1G 51, ^3F 49	60	165	20
$^4H_{13/2}$ 47, ^4I 42, ^2I 11	^3F 96, ^1G 4	309	305	306
$^4I_{11/2}$ 53, ^4H 47	^3F 100	223	207	220
$^4I_{15/2}$ 100	^3F 100	86	70	86

density of states can account for the remaining discrepancy with our expected EA, we performed similar $J=3$ and $J=4$ calculations using DF radial functions and virtual orbitals optimized to the $4f5d^26s$ configuration. Even though there were problems with $4f5d6s^2$ mixing in these calculations, we found that our RCI anion $^4H_{7/2}$ ground state now had an EA of 670 meV or 645 meV when placed relative to the $J=3$ or $J=4$ attachment thresholds, i.e., with similar density of states between the anion and neutral calculations inadequacies in placement of nearby levels tended to cancel out.

Given the above result, it is perhaps fortuitous that the energies of higher J $4f^25d^26s$ thresholds of Pr were not known so that we were forced to reference our bound state from Sec. III D relative to its natural $^6L_{11/2}$ attachment threshold. Otherwise, we may have prematurely declared that state unbound in the early stages of our calculations. On the other hand, test calculations in Gd^- suggest that its lower density of states precludes similar issues with the $6s$ attachments presented in Table III.

More detailed analysis of higher Ce levels found that radial bases optimized to thresholds dominated by singlet terms in the $5d^2$ subgroup had more diffuse $5d$ radial functions, ~0.2 a.u. increase in $\langle r\rangle$, than the states of interest with $5d^2$ ^3F dominant terms. To gauge the error in position of these levels we considered the neutral $J=8$ case where the $^3K_8$ ($5d^2$ ^1G) level was ~225 meV too high relative to the $^5I_8$ ($5d^2$ ^3F) level when compared with the experimental spectrum [10,18]. Moving this level down to its correct position via shifts in the diagonal energy matrix element corresponding to ^3K resulted in negligible impact (0.3 meV) on the position of the ^5I level; the two levels of this high J case are 1.057 eV [10,18] apart with essentially no LS mixing between them. The impact of similar shifts of basis functions with singlet $5d^2$ terms in the anion cases can be seen in the "Shifted BE" column of Table IX with those levels most affected corresponding to those with less $5d^2$ ^3F mixing as indicated in the second column. These values are intended to provide an estimate of possible differences of relative energy positions between anion states if we had the capability to simultaneously optimize our calculations to both $5d^2$ triplet and singlet terms. Again, these values have been adjusted such that the anion ground state matches the expected 660 meV value, and higher J levels that appear to be slightly less bound post-shift have simply been lowered slightly less than the $^4H_{7/2}$ ground state. The important point of this shifted data is that while it appears that predicted positions of some of the weakly bound excited states are perhaps much less accurate than the lower levels, the relative position of the lowest ^5H and ^5I anions states, which were critical to our reinterpretation of the experimental data [7,13], are much more stable.

One final point regarding the uniqueness of Ce is not just its density of states, but its low-lying manifolds that provide thresholds for $6p$ attachments to states other than the LS of its ground state. Even considering the opposite parity Tb and Lu cases presented here, all other lanthanides anion $6p$ attachments of even (odd) parity are attachments to thresholds of the same odd (even) LS manifold. With Ce the ground-state ^1G manifold has a single $J=4$, but there are also low-lying $4f5d6s^2$ ^3F, ^3H, ^3G, and ^1D manifolds with levels beginning at 28 meV, 159 meV, 172 meV, and 294 meV [10,18], respectively. In Table VIII we have included in addition to our usual jj attachment analysis, an LS analysis of the largest terms of the neutral-core portion of the anion wave functions. While there is much LS mixing between Ce neutral thresholds to begin with, it is clear that most of these anion states are not pure attachments to the Ce ground state (55% ^1G, 29% ^3H [10,18]). The same point can be seen in the jj attachment analysis where, for example, in each of the groups of three $J=7/2$ and three $J=9/2$ bound anion states the "(4)" term contributes a total >100%, indicating more than one $J=4$ threshold is contributing to these attachments.

TABLE X. Comparison of RCI lanthanide BEs (meV) for lowest-lying $4f^m5d^26s^2$ anion states with earlier calculations and semiempirical estimates of lanthanide EAs by $5d$ attachment to ground-state configurations. The RCI BE for Ce^- has been shifted to match the experimental LPES data [16], and the Nd^- RCI BE is an estimate scaled from calculations with incomplete RCI bases. The number in parentheses in the "RCI" column is the binding relative to the lowest $4f^m5d^26s$ threshold [10,18]. Note that the earlier values for Pr^- and Nd^- are for $4f^n5d6s^2$ configurations.

Anion	RCI	Calculations	Semiempirical
La^-	545(876)	560 [35]	500 [36]
Ce^-	660(954)	810 [37]	600 [38]
Pr^-	24(856)	110 [37]	300 [38]
Nd^-	−250(841)	100 [37]	100 [38]
Gd^-	70(861)	340 [37]	200 [38]

IV. CONCLUSIONS

While a great leap forward in understanding was made in the early 1990s regarding the identification of the $6p$ attachment to the ground state as the principle mechanism for creation of lanthanide anion states [3,21,25,27,29], it should be noted that earlier work which expected anion states created by $5d$ attachment to lanthanide ground states is directly applicable to our $6s$ attachments to $4f^m5d^26s$ thresholds. In Table X we present some earlier representative calculations and semiempirical estimates, along with our lowest $6s$ attachments from these lanthanides. Note that the configuration is different in the cases of Pr^- and Nd^- where the older work was considering $5d$ attachments to $4f^n6s^2$ ground states, but it is interesting that our selection of possible bound states by considering excited thresholds with open $6s$ subshells would have proved a reasonable indicator of potential bound states for these earlier computational studies. The authors of Ref. [37] indicated that their methodology tended to over-estimate $5d$ binding and suggested that Pr^- and Nd^- were not likely bound despite their calculated EAs of 110 meV and 100 meV. This is consistent with our interpretation considering $6s$ binding of 0.800–0.900 eV relative to Pr $4f^35d6s$ $^6L_{11/2}$ at 1.002 eV or Nd $4f^45d6s$ $^7L_5$ at 1.051 eV [10,18]. We have included our unbound estimate for Nd^- $4f^35d^26s^2$ here to illustrate the nearly uniform binding of $6s$ relative to $4f^m5d^26s$ of 860(20) meV. Of course, Ce^- is the

TABLE XI. Lanthanide anion configurations, number of levels (in parentheses), and lowest level BEs (meV) relative to neutral ground states; $4f^n6s^26p$ cases are from the prior RCI study [2].

	Ground state+$6p$		Excited state+$6s/6p$	
Anion	Configurations	BE	Configurations	BE
La^-	$5d6s^26p$ (8)	434	$5d^26s^2$ (7)	545
Ce^-	$4f5d6s^26p$ (10)	300	$4f5d^26s^2$ (22)	660
Pr^-	$4f^36s^26p$ (6)	177	$4f^25d^26s^2$ (1)	24
Nd^-	$4f^46s^26p$ (7)	167		
Pm^-	$4f^56s^26p$ (8)	154		
Sm^-	$4f^66s^26p$ (8)	130		
Eu^-	$4f^76s^26p$ (6)	117		
Gd^-	$4f^75d6s^26p$ (12)	234	$4f^75d^26s^2$ (3)	70
Tb^-	$4f^96s^26p$ (2)	85	$4f^85d6s^26p$ (6)	88
Dy^-	$4f^{10}6s^26p$ (2)	63		
Ho^-	$4f^{11}6s^26p$ (2)	50		
Er^-	$4f^{12}6s^26p$ (2)	38		
Tm^-	$4f^{13}6s^26p$ (2)	22		
Yb^-				
Lu^-	$4f^{14}5d6s^26p$ (3)	353	$4f^{14}6s^26p^2$ (1)	78

unusual case yet again, but we note that the density of states in the neutral spectrum causes non-negligible mixing of $4f5d^26s$ into lower $4f5d6s^2$ thresholds, possibly enhancing this binding.

The recently developed techniques of universal *jls* restrictions on $4f^{n,m}$ subgroups [1,2] have given us the needed simplification of RCI bases to tackle the most complex lanthanide anions. Together with our earlier study of $6p$ attachments to $4f^n6s^2$ ground states [2] the work presented here represents a complete survey and update of anion states of the entire lanthanide row. In Table XI we present a comprehensive picture of our current understanding of the types of attachments and number of predicted states of each anion, noting that all but Yb^- are predicted to have $6p$ attachments to their ground states, and six lanthanide cases are now predicted to have opposite parity bound states as well. In La^-, Ce^-, and Gd^- the opposite parity states are $5d$ attachments relative to the $4f^m5d6s^2$ ground states but are interpreted here as $6s$ attachments to excited $4f^m5d^26s$ thresholds. This interpretation is bolstered by the Pr^- case where the single opposite parity state does not look like a $5d$ attachment to the $4f^36s^2$ ground state but rather to the $4f^25d6s^2$ configuration. However, the lowest Pr $4f^25d6s^2$ level is $^4I_{9/2}$ at 550 meV [10,18] so one might expect a $5d$ attachment to this $J=9/2$ threshold to have $J=4$ or $J=5$, leaving the best interpretation of our single even $4f^25d^26s^2$ $^5L_6$ Pr^- state as a $6s$ attachment relative to $4f^25d^26s$ $^6L_{11/2,13/2}$. Tb^- and Lu^- have the distinction of opposite parity bound states produced by the same $6p$ attachment mechanism, relative to $4f^85d6s^2$ in Tb and $4f^{14}6s^26p$ in Lu. Finally, La^-, Ce^-, and possibly Tb^- are three cases where the alternate attachment forms the anion ground state.

Errors introduced by the approximations required to deal with midrow lanthanides are difficult to estimate, but comparisons with the "$4f^m$" and "complete" results in Tables V and VII suggest there may be an additional 30–50 meV binding missing from the Gd^- and Tb^- data presented here. Whatever correlation is missed, however, we would expect to contribute nearly equally to the anion states of the same configuration, allowing identification of features in future experimental spectra to shift all the RCI BEs of a particular anion parity by a common amount. Given our thorough exploration of attachment thresholds as presented in Table I, we do not expect that there are any further bound lanthanide anion configurations. At most we expect that adjustment of BEs by future experimental analyses will slightly increase or decrease the number of bound states in any given anion. Even with this completion of our survey of lanthanide anion states there is more computational work to be done, e.g., calculation of photodetachment partial cross sections [1,7] to aid in understanding of features of experimental spectra. While we certainly encourage any experimental interest in continued lanthanide photodetachment studies, there are also opportunities for further examination of the neutral lanthanide thresholds presented in Table I (our RCI *LS* analysis is most useful in predicting strong photodetachment channels in cases where the final state threshold composition is also known). For example, the current experimental analysis of level composition of neutral Ce is incomplete for thresholds above ~1.3 eV [10,18], which is well within the photon energies used by typical LPES experiments [13,16].

ACKNOWLEDGMENTS

Support for this work from the National Science Foundation, Grant No. PHY-0097111, is gratefully acknowledged.

[1] S. M. O'Malley and D. R. Beck, Phys. Rev. A **77**, 012505 (2008).
[2] S. M. O'Malley and D. R. Beck, Phys. Rev. A **78**, 012510 (2008).
[3] K. Dinov, D. R. Beck, and D. Datta, Phys. Rev. A **50**, 1144 (1994).
[4] P. L. Norquist and D. R. Beck, Phys. Rev. A **61**, 014501 (1999).
[5] S. M. O'Malley and D. R. Beck, Phys. Rev. A **65**, 064502 (2002).
[6] X. Cao and M. Dolg, Phys. Rev. A **69**, 042508 (2004).
[7] S. M. O'Malley and D. R. Beck, Phys. Rev. A **74**, 042509 (2006).
[8] C. S. Feigerle, R. R. Corderman, S. V. Bobashev, and W. C. Lineberger, J. Chem. Phys. **74**, 1580 (1981).
[9] M.-J. Nadeau, M. A. Garwan, X. L. Zhao, and A. E. Litherland, Nucl. Instrum. Methods Phys. Res. B **123**, 521 (1997).
[10] Yu. Ralchenko, A. E. Kramida, J. Reader, and NIST ASD Team, NIST Atomic Spectra Database (version 3.1.5), available at http://physics.nist.gov/asd3, National Institute of Standards and Technology, Gaithersburg, MD, 2008.
[11] J. E. Sansonetti, W. C. Martin, and S. L. Young, NIST Handbook of Basic Atomic Spectroscopic Data (version 1.1.2), available at http://physics.nist.gov/PhysRefData/Handbook, National Institute of Standards and Technology, Gaithersburg, MD,2008.
[12] C. S. Feigerle, Z. Herman, and W. C. Lineberger, J. Electron Spectrosc. Relat. Phenom. **23**, 441 (1981).
[13] V. T. Davis and J. S. Thompson, Phys. Rev. Lett. **88**, 073003 (2002).
[14] S. M. O'Malley and D. R. Beck, Phys. Rev. A **60**, 2558 (1999).
[15] S. M. O'Malley and D. R. Beck, J. Phys. B **33**, 4337 (2000).
[16] A. M. Covington, D. Calabrese, J. S. Thompson, and T. J. Kvale, J. Phys. B **31**, L855 (1998).
[17] V. T. Davis and J. S. Thompson, J. Phys. B **34**, L433 (2001).
[18] *Atomic Energy Levels—The Rare-Earth Elements*, edited by W. C. Martin, R. Zalubas, and L. Hagan, Natl. Bur. Stand. Ref. Data Ser. Natl. Bur. Stand. (U. S.) Circ. No. 60 (U.S. GPO, Washington, DC, 1978).
[19] V. T. Davis, J. S. Thompson, and A. Covington, Nucl. Instrum. Methods Phys. Res. B **241**, 118 (2005).
[20] C. W. Walter, N. D. Gibson, C. M. Janczak, K. A. Starr, A. P. Snedden, R. L. Field III, and P. Andersson, Phys. Rev. A **76**, 052702 (2007).
[21] E. Eliav, U. Kaldor, and Y. Ishikawa, Phys. Rev. A **52**, 291 (1995).
[22] J. P. Desclaux, Comput. Phys. Commun. **9**, 31 (1975).
[23] F. A. Parpia, C. Froese Fischer, and I. P. Grant, Comput. Phys. Commun. **94**, 249 (1996).
[24] P. Jönsson, X. He, C. Froese Fischer, and I. P. Grant, Comput. Phys. Commun. **177**, 597 (2007).
[25] K. Dinov and D. R. Beck, Phys. Rev. A **51**, 1680 (1995).
[26] V. T. Davis and J. S. Thompson, J. Phys. B **35**, L11 (2002).
[27] S. H. Vosko and J. A. Chevary, J. Phys. B **26**, 873 (1993).
[28] Z. Felfli, A. Z. Msezane, and D. Sokolovski, Phys. Rev. A **78**, 030703(R) (2008).
[29] S. H. Vosko, J. B. Lagowski, I. L. Mayer, and J. A. Chevary, Phys. Rev. A **43**, 6389 (1991).
[30] D. Berkovits, E. Obaretto, M. Paul, and G. Hollos, Rev. Sci. Instrum. **63**, 2825 (1992).
[31] M. A. Garwan, A. E. Litherland, M. J. Nadeau, and X. L. Zhao, Nucl. Instrum. Methods Phys. Res. B **79**, 631 (1993).
[32] D. Berkovits, S. Ghelberg, O. Heber, and M. Paul, Nucl. Instrum. Methods Phys. Res. B **123**, 515 (1997).
[33] S. M. O'Malley and D. R. Beck, Phys. Rev. A **61**, 034501 (2000).
[34] Z. Felfli, A. Z. Msezane, and D. Sokolovski, J. Phys. B **41**, 1 (2008).
[35] K. D. Sen, P. C. Schmidt, and A. Weiss, J. Chem. Phys. **75**, 1037 (1981).
[36] H. Hotop and W. C. Lineberger, J. Phys. Chem. Ref. Data **14**, 731 (1985).
[37] L. A. Cole and J. P. Perdew, Phys. Rev. A **25**, 1265 (1982).
[38] R. Zollweg, J. Chem. Phys. **50**, 4251 (1969).